Model for eutectic organization: The purely kinetic regime

C. Misbah and D. E. Temkin*
Laboratoire de Spectrométrie Physique, Université Joseph Fourier, Grenoble I, Boîte Postale 87, 38402 Saint-Martin d'Hères, Cedex, France
(Received 6 October 1993)

We analyze the lamellar organization in the solid phase by using a purely kinetic regime based on physical first principles combined with a phenomenological Landau theory. This model has at least two advantages over the usual free-boundary-problem formulation: (i) It allows us to show from first principles the existence of a lamellar organization, which is usually taken as a starting point, and (ii) it permits us to handle analytically in a relatively simple manner the problem of the existence of these solutions. This model resembles in some way the phase-field model: the solid-fluid front is sharp, while the solid-solid interface is smooth and characterized by a continuous change in the concentration field. We analyze in detail the variety of solutions and map them to the underlying coexistence phase diagram of the three phases. We show that the growing phase with a modulated structure (the "lamellar" eutectic structure) has a higher velocity than any homogenous solution. The organized structure thus appears from the maximum-velocity principle as favorable against homogeneous solutions. Other questions related to various symmetry-breaking bifurcations from the simplest steady and symmetric organization are discussed, where use of the present model may become essential.
PACS number(s): 61.50.Cj

I. INTRODUCTION

There has been during the past decade an increasing interest in the problem of pattern formation of a moving boundary, such as a solidification front. The discovery of a myriad of fascinating patterns has stimulated an impressive revival of the field and has even suggested various investigations about their relevance to more complex phenomena such as those encountered in natural systems. There continues to be a need, however, for simple models with the aim to get more insight towards the understanding of the intricate nature of the mechanism by which a pattern can spontaneously be formed.

The eutectic system is an active branch in pattern formation and has recently known an impressive renewed interest both experimentally [1,2] and theoretically [3–6]. There are several reasons. For example, most solidification microstructures are usually either dendritic or eutectic. Generically, the phase diagram of two substances mixed together has a eutectic point, since the theoretical critical temperature for phase separation in the solid phase (at low temperature where enthalpy prevails over entropy) is above the (generic) azeotropic point. The presence of an azeotropic feature follows from the fact that mixing in the solid costs a large stress energy. The eutectic system is, on the other hand, the first step beyond a pure substance (or a very dilute solution), which is often the exception rather than the rule in real systems. Eutectics can be thought of as the simplest passive multi-component systems, in the sense that the growth does not involve reaction. Even in such a case we lack a full understanding of the patterns that may arise.

Since Jackson and Hunt [7] showed that the free-boundary problem admits a whole family (parametrized by the wavelength) of steady-state periodic solutions, work on the eutectic system has advanced considerably [3–6,8], revealing a variety of other solutions. The investigations often involve, however, heavy and sophisticated numerical techniques of the nonlocal and retarded front equation. A simple but physically relevant model would therefore be highly desirable.

In this paper we propose such a model. This model is akin to the widely used phase-field model [9, 10]. Let us recall that the usual phase-field model for a binary system [10] consists of introducing two fields: "the phase transformation field" (which describes the transition between liquid and solid), and the composition field. Our main concern in this paper is to describe the lamellar organization in the solid phase. In a simplified picture, our model will be characterized by a *single* field, describing the composition distribution in the growing phase. Of course, eutectic growth usually results from a cooperative diffusive phenomenon between the adjacent regions ahead of the front. In principle, then, we should introduce a composition field in the liquid phase, as well. We shall not include this complication here. Rather, we make the assumption that the concentration in the liquid (or fluid in general) phase is kept constant, so that we focus only on the solid composition to see whether the growing phase organizes in a lamellar structure or not (and possibly in more complicated structures; see later). If the cooperative phenomenon is suppressed from the model, another ingredient must be added to ensure the solidification process. This is the kinetic attachment of molecules to the interface, which becomes relevant if the liquid phase has

*Permanent address: I. P. Bardin Institute for Ferrous Metals, Moscow 107005, Russia.

a uniform composition (as we assume). This regime is attained at high velocity when the freezing time, given by d/V, where V is the growth velocity and d the liquid-solid extent, is of the order of the mass diffusion time, given by D/V^2, D being the diffusion constant. By taking typical values $d \sim 10$ Å and $D \sim 10^{-5}$ cm^2/s, we find that the kinetical regime is attained for velocities of the order of 1 m/s, which are by now accessible velocities in rapid solidification experiments which use a pulsed laser. It is also possible to imagine *artificial* means to reach this regime. This situation could in principle be achieved in, at least, two ways: (i) By strongly stirring the liquid phase so that the hydrodynamic boundary layer becomes small on the scale of wavelength of interest, and (ii) by considering the growth from a turbulent gas. We shall consider, moreover, the transition width across the fluid-solid interface to be infinitely small. The condition across the front reduces thus to a usual free-boundary condition.

This paper is organized as follows. In Sec. II, we present the model and introduce appropriate scales to make the equations dimensionless. In Sec. III, we look for steady-state solutions, both homogenous and modulated. In Sec. IV, we present the overall picture on steady growth. Section V is devoted to discussion of the results and to speculations about more complex structures. Section VI contains the conclusion.

II. THE MODEL EQUATIONS

We consider that the fluid, whose composition is kept constant, has prescribed chemical potentials μ_{FA} and μ_{FB} for the two components A and B of the alloy. The net mass fluxes J_A and J_B across the fluid-solid (from the fluid into the solid) interface are defined as

$$J_A = W_A(\mu_{FA} - \mu_{SA}), \quad J_B = W_B(\mu_{FB} - \mu_{SB}), \tag{1}$$

where μ_{SA} and μ_{SB} are the chemical potentials in the solid phases (to be defined below), and W_A and W_B are phenomenological kinetic coefficients. Note that we consider small departures from equilibrium, a situation which is often fulfilled for molecularly rough interfaces and that we disregard cross terms. The growth velocity v_n (only its normal component enters), and the composition $c(x,\ t)$, of the growing solid, are related to mass fluxes by

$$J_A = (1-c)v_n, \quad J_B = cv_n. \tag{2}$$

The main point of the model is to write the functional relation between the chemical potentials μ_{SA}, μ_{SB}, and the solid composition field c. Since we are interested in the solid organization we consider that the composition is independent of the z coordinate (which is the coordinate along the growth axis). The functional relations are then given by [11]

$$\mu_{SA} = f_s(c) - c\frac{\partial f_s}{\partial c} - \frac{1}{2}\alpha c'^2 + \alpha c c'' + \sigma\Omega\kappa\ , \tag{3}$$

$$\mu_{SB} = f_s(c) + (1-c)\frac{\partial f_s}{\partial c} - \frac{1}{2}\alpha c'^2 - \alpha(1-c)c'' + \sigma\Omega\kappa\ , \tag{4}$$

where $f_s(c)$ is the free energy per atom for a homogeneous solid phase, and α is a wall energy parameter which enters the total free energy à la Cahn and Hilliard [12],

$$F = \Omega^{-1}\int [f_s + \tfrac{1}{2}\alpha c'^2]d\Omega, \tag{5}$$

where the integration is performed over the solid phase and the prime designates derivative with respect to x. We have included in Eqs. (3) and (4) the Gibbs-Thomson corrections to the chemical potential, where κ is the front curvature (taken as positive for a convex profile), σ is the surface energy, and Ω is the atomic volume.

In order to keep the analysis simple, we shall confine ourselves to the symmetric model: the A-rich and B-rich phases have exactly the same properties, and the fluid composition is kept at the value 1/2,

$$W_A = W_B \equiv W, \quad \mu_{FA} = \mu_{FB} \equiv \mu_F. \tag{6}$$

In order to allow for a thermodynamical instability leading potentially to phase separation of the solid phase, f_s is taken to have the generic form (Fig. 1)

$$f_s = f_0 - \tilde{a}\tilde{\eta}^2 + \tilde{b}\tilde{\eta}^4, \quad \tilde{\eta} \equiv c - \tfrac{1}{2}, \tag{7}$$

where f_0, $\tilde{a}$, and $\tilde{b}$ are phenomenological Landau parameters. We find it convenient to introduce dimensionless quantities. For that purpose, we introduce

$$\begin{aligned} &\text{length scale}: \ l_c = \sqrt{\alpha/\tilde{a}}, \\ &\text{concentration scale}: \ \eta_e = \sqrt{\tilde{a}/2\tilde{b}}, \\ &\text{velocity scale}: \ V_s = W\tilde{a}^2/4\tilde{b}, \\ &\text{energy scale}: \ E_s = \tilde{a}^2/4\tilde{b}. \end{aligned} \tag{8}$$

Note that $\pm\eta_e$ correspond to the usual equilibrium composition of the two solid phases (at a given temperature) and l_c is the characteristic width of the boundary between the two phases (e.g., the α and β phases in the eutectic system).

Substituting (7) into (3) and (4), and making use of 1 and 2, it is a simple matter to write a set of two coupled equations for the unknown quantities, $\eta(x,t)$ (the reduced solid composition) and the fluid-solid profile $\zeta(x,t)$:

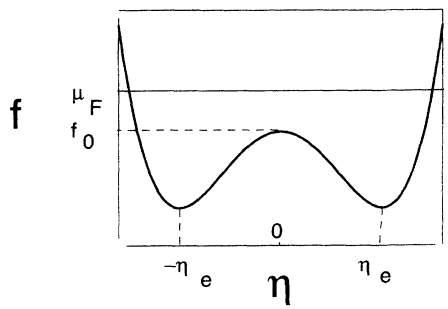

FIG. 1. A schematic plot of the free energy.

$$a\eta\left(\Delta + 2\eta^2 - \eta^4 + \eta'^2 + \frac{d_0\zeta''}{(1+\zeta'^2)^{3/2}}\right)$$

$$+(2a\eta^2+1)(2\eta^3 - 2\eta - \eta'') = 0, \quad (9)$$

$$\frac{V+\dot{\zeta}}{2\sqrt{1+\zeta'^2}} = \Delta - 2\eta^2 + 3\eta^4 + \eta'^2 - 2\eta\eta''$$

$$+\frac{d_0\zeta''}{(1+\zeta'^2)^{3/2}}\,, \quad (10)$$

where

$$\Delta = \frac{\mu_F - f_0}{E_s}, \quad d_0 = \frac{\sigma\Omega}{l_c E_s}, \quad a = \frac{\tilde{a}}{\tilde{b}}. \quad (11)$$

Note that all other quantities appearing in (9) and (10) (e.g., ζ, V, ...), have been scaled by the quantities defined in Eq. (8). The quantity Δ in Eq. (11) plays the role of a reduced driving force.

III. STEADY-STATE SOLUTIONS

We shall deal in this section with simple steady-state solutions of Eqs. (9) and (10). We distinguish between homogeneous and modulated solutions.

A. Homogeneous steady-state solutions

These solutions correspond to a planar front moving at a constant speed V, with a constant solid composition η_0 to be determined below. It is easy to see that Eqs. (9) and (10) have two such solutions:

$$V = 2\Delta\,, \quad \eta_0 = 0\,, \quad (12)$$

$$V = \frac{4}{a}(1-\eta_0^2)\,,$$

$$\eta_0^2 = \frac{1}{3}[1 - a^{-1} + \sqrt{(a^{-1}-1)^2 + 3(2a^{-1}-\Delta)}]\,. \quad (13)$$

Figures 2(a) and 2(b) display the behavior of V and η_0 as functions of the driving force Δ. Solution (12) exists for all $\Delta > 0$ (i.e., for $\mu_F > f_0$; note that f_0 is the maximum in Fig. 1), while solution (13) exists only in the interval $0 < \eta_0^2 < 1$, which amounts to $-1 < \Delta < 2a^{-1}$. At large enough supersaturation, only the trivial solution ($\eta_0 = 0$) survives. By lowering the supersaturation, a new branch [$\eta_0 \neq 0$; Eq. (13)] branches off the trivial solution at the bifurcation point $\Delta = 2a^{-1}$ (see Fig. 2). The nontrivial solution ceases to exist at $\Delta = -1$, which corresponds to the usual thermodynamical equilibrium between three phases (the eutectic point).

A linear stability analysis shows that both homogeneous solutions are stable.

B. Spatially modulated solutions

An interesting question is whether Eqs. (9) and (10) support modulated solutions characterized by a spatially varying composition $\eta(x)$ and a front profile $\zeta(x)$. In general, answering such a question requires a numerical integration. Rather than resorting to "brute force," we wish to push further the analytical analysis. To do so, some approximation is necessary. We assume that front depletion is small enough so that we can neglect ζ'^2 in the square root entering in the left-hand side of Eq. (10) and in the curvature. In the next section, we discuss in some detail the condition under which such an assumption is permissible.

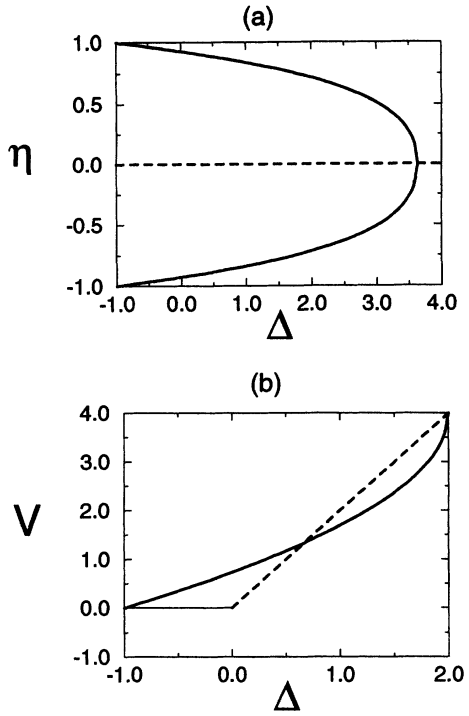

FIG. 2. (a) The behavior of the solid composition as a function of the driving force Δ. (b) The behavior of the growth velocity as a function of Δ. The dashed line represents the trivial solution ($\eta_0 = 0$), while the full line represents the nontrivial one ($\eta \neq 0$). We have taken $a = 1$.

Given the above assumption, Eqs. (9) and (10) can be decoupled. Multiply Eq. (10) by $a\eta$ and subtract it from Eq. (9). The result is

$$\eta'' + 2\eta - 2\eta^3 - \frac{a\eta V}{2} = 0\,, \quad (14)$$

which constitutes a closed equation for η, parametrized by the growth velocity V. This equation is analogous to that of an anharmonic oscillator without dissipation, where x plays the role of time. This remark will be useful later. Once $\eta(x)$ is determined we can deduce $\zeta(x)$ from Eq. (9), which gives

$$-d_0\zeta'' = \Delta - 2\eta^2 + 3\eta^4 + \eta'^2 - 2\eta\eta'' - \frac{V}{2}\,. \quad (15)$$

The simplest modulated structure corresponds to a periodic solution. In order to investigate its existence, we proceed as follows: Equation (14) has the first integral

$$\eta'^2 = -2\left(1 - \frac{aV}{4}\right)\eta^2 + \eta^4 + A, \tag{16}$$

where A is an integration constant. Equation (16) is analogous to that of an anharmonic oscillator without dissipation, where A plays the role of the total energy. More precisely we can rewrite Eq. (16) as

$$E_k + E_p = A\ , \tag{17}$$

where

$$E_k = \eta'^2, \quad E_p = 2\left(1 - \frac{aV}{4}\right)\eta^2 - \eta^4 \tag{18}$$

represent the analogues of the kinetic and potential energy, respectively, and x plays the role of time. In order that the system exhibit oscillations, we must have $V < 4/a$, a condition which ensures the existence of a local minimum in the potential energy. Moreover the total energy must be positive, but smaller than the maximum value of the potential energy which is easily found to be $(1 - aV/4)^2$. Oscillations are then possible under the conditions

$$V < \frac{4}{a}, \quad 0 < A < \left(1 - \frac{aV}{4}\right)^2. \tag{19}$$

The maximum amplitude of oscillations is attained when the kinetic energy vanishes. When condition (19) holds, we can write Eq. (16) as

$$\eta'^2 = -2\left(1 - \frac{aV}{4}\right)\eta^2 + \eta^4 + A \equiv (\eta^2 - \eta_1^2)(\eta^2 - \eta_2^2), \tag{20}$$

where

$$\eta_{1,2}^2 = 1 - \frac{aV}{4} \mp \sqrt{\left(1 - \frac{aV}{4}\right)^2 - A}\ . \tag{21}$$

We obviously have the inequality

$$0 \le \eta_1^2 \le \eta_2^2\ . \tag{22}$$

It is seen from Eq. (20) that the kinetic energy vanishes at $\eta = \pm\eta_1$ and $\eta = \pm\eta_2$. Since oscillations are possible around the minimum potential energy only, we conclude that the oscillation amplitude is η_1. More precisely the modulated solution is characterized by oscillations of $\eta(x)$ between η_1 and $-\eta_1$ (see below). Figure 3 summarizes the analogy with the anharmonic oscillator.

Let λ denote the (dimensionless) periodicity of the structure. Then integrating Eq. (16) from 0 to $\lambda/2$ (where η varies from η_1 to $-\eta_1$), we obtain

$$\lambda = \frac{4}{\eta_2} K(\eta_1/\eta_2)\ , \tag{23}$$

where K stands for the complete elliptic integral. Equation (23) provides a relation between the constant of integration A, λ, and V. A second relation can be obtained by exploiting Eq. (14). Using Eq. (15) we can rewrite Eq. (14) as

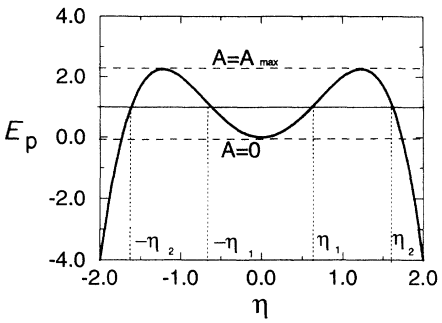

FIG. 3. A schematic view on the analogy with the anharmonic oscillator. Oscillations take place between $-\eta_1$ and η_1. For $A = 0$ (A is the total energy) there is no oscillation: the system will spend an infinite time in the position $\eta = 0$, a situation which corresponds to the trivial homogeneous solution represented by the dashed line in Fig. 2. For $0 < A < A_{\max} \equiv (1 - aV/4)^2$ there are oscillations. In the extreme limit $A = A_{\max}$ the system is initially, say, at $\eta = -\eta_1$ (in this case we have a degeneracy: $\eta_1 = \eta_2$), and will move to the position $\eta = \eta_1$ after an infinite time. The stay time is logarithmically diverging (see Eq. (30)]. This solution is the one represented by the full line in Fig. 2.

$$-d_0\zeta'' = \Delta - \frac{V}{2} + A - \frac{aV}{2}\eta^2\ . \tag{24}$$

Integrating this equation from $x = 0$ to $x = \lambda/2$, and using $dx = d\eta/\eta'$ together with Eq. (20), we obtain

$$\frac{2}{\eta_2}\left(\Delta - \frac{V}{2} + A\right)K(\eta_1/\eta_2)$$

$$-aV\eta_2[K(\eta_1/\eta_2) - E(\eta_1/\eta_2)] = 0\ , \tag{25}$$

where E designates the complete elliptic integral of the second kind. For a fixed Δ, Eqs. (23) and (25) provide A and V as functions of λ, which we are first going to investigate in some limiting cases, and a comparison with the usual free-boundary problem will be given.

A nonmoving front

An instructive case is the one where the solid-fluid front is not moving ($V = 0$). In this case Eq. (21) becomes

$$\eta_{1,2} = 1 \mp \sqrt{1 - A}\ , \tag{26}$$

while Eq. (25) yields (upon using the properties of the elliptic functions)

$$A = -\Delta\ . \tag{27}$$

The periodicity λ is obtained from Eq. (23),

$$\lambda = \frac{4}{\sqrt{1 + \sqrt{1 + \Delta}}} K\left(\sqrt{\frac{1 - \sqrt{1 + \Delta}}{1 + \sqrt{1 + \Delta}}}\right)\ . \tag{28}$$

This solution corresponds to a situation where a fluid is in equilibrium with a solid having a modulated composition

and with a periodicity given by Eq. (28). Obviously, this solution exists in the range $\Delta \in [-1, 0]$, a domain which corresponds to the one between the minimum and the maximum in Fig. 1.

Using the properties of the elliptic functions, it is easy to identify from (28) the two extreme limits

$$\Delta \to 0\,, \quad \lambda \simeq \pi\sqrt{2}\left(1 - \frac{3\Delta}{16}\right)\,, \quad \eta_1 \simeq \sqrt{\frac{-\Delta}{2}}\,, \tag{29}$$

$$\Delta \to -1\,, \quad \lambda \simeq 4\ln\left(\frac{2\sqrt{2}}{(1+\Delta)^{1/4}}\right)\,,$$

$$\eta_1 \simeq 1 - \frac{\sqrt{1+\Delta}}{2}\,. \tag{30}$$

In the first case the structure is modulated with a finite wavelength and a small amplitude η_1, while in the second case we approach the equilibrium concentration ($\eta = 1$ in reduced units) with a logarithmically diverging wavelength. Note that Eq. (29) represents a limit to the dashed curve in Fig. 2(b), where there the solution is homogeneous (η is independent on x). The case of Eq. (30) shows that we tend to a homogeneous solution, the one represented by a solid line in Fig. 2.

IV. THE OVERALL PICTURE OF STEADY STATES

As stated in the preceding section, Eqs. (23)–(25) are the main results for steady growth, that we would like to treat in detail here. These are two equations for the unknowns Δ, V, λ, A. This means that the total number of degrees of freedom is equal to 2. One of the two equations serves to determine A as a function of Δ, V, λ. The second one gives a relation between these three parameters, as in the usual formulation of eutectic growth. In free growth, the supersaturation Δ is a quantity that is fixed by the operator. We are left then with two parameters λ and V which are related to each other. Our strategy is then to fix Δ and determine the couple A and V for each wavelength from Eqs. (23)–(25). This provides us with series of curves $V(\lambda)$ parametrized by the supersaturation. The computation involves a standard Newton-Raphson scheme for solving the two nonlinear algebraic equations. Figure 4 displays the behavior of V as a function of λ. Some remarks are in order. The curve $V(\lambda)$ takes on a maximum at a particular value of λ. On the other hand, V vanishes below some critical value of λ which is typically the nucleation radius. The behavior is similar to that obtained in the usual eutectic formulation. The existence of a maximum velocity growth raises the possibility that that state is the actually selected one. We do not believe, however, that such a principle holds exactly. Nonetheless, its consequences have been explored—and often supported—in the metallurgical literature [13].

At this point we have not yet answered an important question: what discriminates between the homogeneous solutions discussed in Sec. III A and the modulated one.

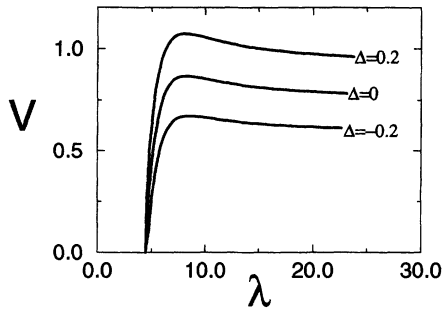

FIG. 4. The growth velocity V as a function of the wavelength for various supersaturations. Here $a = 1$.

For that purpose, we evaluated the maximum growth velocity for each supersaturation, and compared these velocities to those presented in Fig. 2(b). Our results are summarized in Fig. 5. There, besides the two homogeneous solutions (the solid and dashed lines), we plot (dashed-dotted line) the maximum velocity for the modulated structure. An interesting result emerges here: the modulated structure has a higher velocity than the homogeneous ones in the range $\Delta \in [-1, 2a^{-1}]$. If we admit the usual maximum velocity principle—the fastest pattern wins—the modulated structure should prevail if the supersatuation is not too high. Beyond $\Delta = 2a^{-1}$ (or equivalently $V = 4a^{-1}$) there is no modulated structure at all, and the only solution that survives is the trivial homogenous solution ($\eta = 0$). This is consistent with our condition (19). In some sense, when the supersaturation is too high, the fluid is frozen at its nominal composition in the solid phase.

The solution of Eq. (16) can easily be expressed in terms of an incomplete elliptic integral [14]. We represent in Fig. 6(a) the typical behavior of the concentration in the solid phase, which shows a modulation from $-\eta_1$ to η_1, characterizing the lamellar structure. Once $\eta(x)$ is determined, a simple integration of the second order equation (24) yields the front profile displayed in Fig. 6(b). We have included vertical lines as guides to the eye

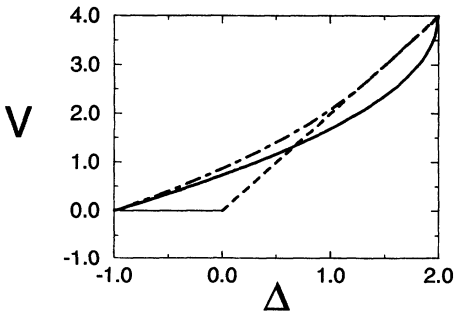

FIG. 5. The growth velocity as a function of the driving force. The trivial homogeneous solution (dashed line), the nontrivial homogeneous solution (full line), and the periodic solution where the maximum velocity is taken as the actual growth speed (dashed-dotted line). Here $a = 1$.

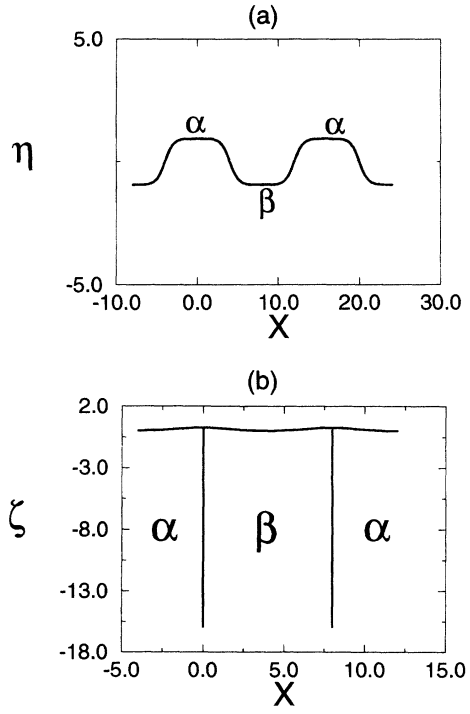

FIG. 6. (a) A typical behavior of $\eta(x)$ for the periodic solution. (b) A typical front profile. Here $a = 1$, $d_0 = 1$, and $\Delta = -0.6$.

in order to easily distinguish between the two lamellae.

The determination of these quantities has been made under the assumption that the front depletion is small so that we kept only the leading terms in ζ. We would like to discuss this assumption now. Since our aim is to give a rough estimate, we shall analyze the two sets of Eqs. (9) and (10) in a limit where a full analytical analysis is possible. This is the case where $\eta_1 = \eta_2$. In this case the modulation is infinitely long [see Eq. (23); $K(1) = \infty$, while $A = (1 - aV/2)$ from Eq. (25)]. This allows us to obtain from Eq. (16) an explicit form for $\eta(x)$,

$$\eta(x) = \sqrt{1 - \frac{aV}{4}} \tanh\left(x\sqrt{1 - \frac{aV}{4}}\right) . \tag{31}$$

The determination of the front profile $\zeta(x)$ is straightforward from Eq. (10)

$$\zeta(x) = -\frac{aV}{2d_0}\ln[\cosh(\eta_0 x)] , \tag{32}$$

where we recall that η_0 is the composition of the homogeneous solution [see Eq. (13)]. The maximum value of ζ', $\zeta'_{\max}$, is $\zeta'_{\max} = aV\eta_0/(2d_0) = 2\eta_0(1 - \eta_0^2)/d_0$, where use has been made of Eq. (13). We should now determine the value of η_0 that provides the maximum ζ'. We maximize ζ' by differentiation with respect to η_0 to find

$$\zeta'_{\max} = \frac{4}{3\sqrt{3}d_0} . \tag{33}$$

In conclusion, the assumption $\zeta' << 1$ amounts to $d_0 >> 1$. From the definition (11), $d_0 \sim (E_F/E_s)(l/l_c)$, where E_F is the fluid-solid surface energy, and l is an atomic distance. Recall that E_s is the solid-solid wall energy, and l_c is the wall width, so that typically $d_0 \sim 1$. Since we cannot be certain how valid our assumption is, we have solved the full equations with $d_0 = 1$. Although there are variations of up to 30%, the overall picture of our findings remains unaltered.

V. CONCLUSION AND OUTLOOK

We have presented an extremely simple version of eutectic growth in the kinetic regime, which has allowed us to deal with many points analytically, or by using elementary numerical methods. This analysis has allowed us to capture the essential results. A feature found here is that a modulated pattern has a higher growth velocity than homogenous ones, a fact which provides an out-of-equilibrium explanation for the observation, in standard experiments, of lamellar eutectic growth rather than homogeneous growth. However, at large enough supersaturation, the modulated pattern ceases to exist, while the fastest growth is a homogenous one. This feature may be related to the experimental observation [15] that above a certain supersaturation, a homogeneous plane front emerges from the initially lamellar structure before *cyclic* dynamics take place, leading ultimately to a banded structure.

Before concluding, let us make some remarks which are pertinent to future investigations. It is now well known that the eutectic system possesses a variety of solutions

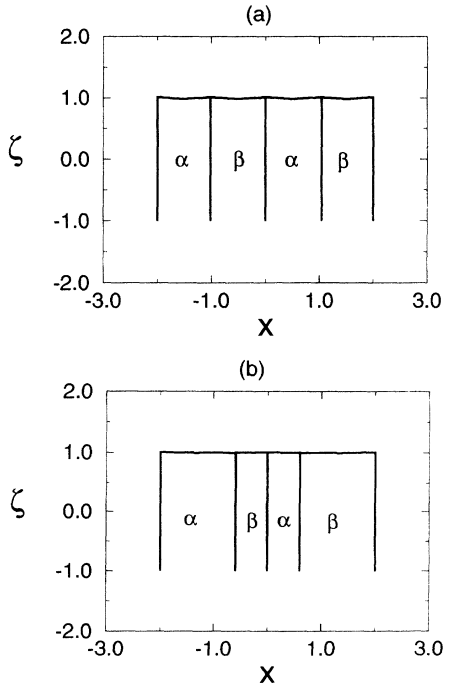

FIG. 7. (a) The case where the extent of the α and β phases are the same. Here we have two periods. (b) The case where the symmetry is broken: the period has doubled. Both cases are schematic.

[5]. Among them are the broken-parity solutions, the vacillating-breathing oscillatory mode, the optical one, etc. reported on in many situations. Another promising line of investigation concerns the fundamental question of *the existence of wavelength selection.* For example, the full free-boundary formulation shows that for a symmetric phase diagram (where the α and β phases are equivalent, as considered here) the pattern suffers a new type of symmetry-breaking [16] bifurcation resulting in a pattern consisting of a large α lamella of extent L, followed by a thin β one of extent l, then a thin α one with an extent l and again a large β one with an extent L and so on, as schematically shown in Fig. 7(b). If we take the case $L = l$ as a starting point [Fig. 7(a)], then we are in a situation where the pattern undergoes a *spatial period-doubling bifurcation* (Fig. 7(b)]. More complicated patterns than the subharmonic cascade (where the wavelength of the bifurcating state is generically irrationally related to that of the mother state) are also possible [16]. There are also hints [16] for the existence, within the full formulation, of a second *spatial period-doubling cascade* (or a more complicated *irrational* cascade), and it is likely that this scenario repeats itself *ad infinitum.* All the bifurcations may accumulate [16] close to the minimum undercooling point (or equivalently close to the maximum velocity point). This means that the apparently selected state reported on in many experiments (which corresponds—at least approximately—to the maximum velocity) is close (in parameter space) to an *infinite* set of attractors, which is a signature of the *fragility* of the apparently periodic state against a *spatially disordered one.* These questions, among many others, are now being investigated within the current model, which contains enough essential physical ingredients to expect rich dynamics to occur. Since any analytical or numerical effort becomes increasingly complex within the usual free-boundary formulation, the model presented here is a promising candidate on which to study the various patterns. We hope to report along these lines in the near future.

[1] G. Faivre, S. de Cheveigné, C. Guthmann, and P. Kurowski, Europhys. Lett. **9**, 779 (1989); G. Faivre and J. Mergy, Phys. Rev. A **45**, 7320 (1992); B. Caroli, C. Caroli, G. Faivre, and J. Mergy, J. Cryst. Growth **118**, 135 (1992); G. Faivre and J. Mergy, Phys. Rev. A **46**, 963 (1992).

[2] V. Seetharaman and R. Trivedi, Metall. Trans. **19A**, 2955 (1988).

[3] A. Karma, Phys. Rev. Lett. **59**, 71 (1987).

[4] K. Brattkus, B. Caroli, C. Caroli, and B. Roulet, J. Phys. (Paris) **51**, 1847 (1990); B. Caroli, C. Caroli, and B. Roulet, *ibid* **51**, 1865 (1990).

[5] K. Kassner and C. Misbah, Phys. Rev. Lett. **65**, 1458 (1990); **66**, 522(E) (1991); **66**, 445 (1991); Phys. Rev. A **44**, 6513 (1991); **44**, 6533 (1991); C. Misbah and D.E. Temkin, *ibid.* **46**, 4497 (1992); K. Kassner, A. Valance, C. Misbah, and D.E. Temkin, Phys. Rev. E **48**, 1091 (1993).

[6] R.-F. Xiao, J.I.D. Alexander, and F. Rosenberger, Phys. Rev. A **45**, 571 (1992).

[7] K.A. Jackson and J.D. Hunt, Trans. Metall. Soc. AIME **236**, 1129, (1966).

[8] J.S. Langer, Phys. Rev. Lett. **44**, 1023 (1980); V. Datye and J.S. Langer, Phys. Rev. B **24**, 4155 (1981).

[9] See, for example, R. Kobayashi, Bull. Jpn. Soc. Ind. Appl. Math. **1**, 22 (1991).

[10] A.A. Wheeler, W.J. Boettinger, and G.B. McFadden, Phys. Rev. A **45**, 7424 (1992); A. Karma (unpublished).

[11] E.A. Brener and D.E. Temkin, Sov. Phys. Crystallogr. **30**, 140 (1985).

[12] J. W. Cahn and J.E. Hilliard, J. Chem. Phys. **31**, 688 (1958).

[13] See, for example, G. Lesoult, Ann. Chim. Paris **5**, 154 (1980).

[14] *Handbook of Mathematical Functions,* edited by M. Abramowitz and I.A. Stegun (Dover, New York, 1972).

[15] M. Carrard, M. Gremaud, M. Zimmermann, and W. Kurz, Acta Metall. **40**, 983 (1992).

[16] C. Misbah and D.E. Temkin (unpublished).